Nanoscale Advances

ROYAL SOCIETY OF CHEMISTRY

PAPER

View Article Online
View Journal | View Issue

Cite this: *Nanoscale Adv.*, 2026, **8**, 2246

First principles investigation of the ferromagnetism in TM-doped arsenene monolayer (TM = Mn and Fe)

Pham Minh Tan,[a] Nguyen Thanh Son,[b] R. Ponce-Pérez,[c] Duy Khanh Nguyen,[de] J. Guerrero-Sanchez[c] and D. M. Hoat[*fg]

Because of lacking intrinsic magnetism, developing efficient methods for the magnetism engineering in two-dimensional (2D) materials is necessary in order to make new spintronic materials. In this work, doping and codoping with transition metals (TMs = Mn and Fe) is proposed to modify the arsenene monolayer electronic and magnetic properties. Bare monolayer is intrinsically nonmagnetic, exhibiting semiconductor character with an indirect gap of 1.60 eV. Mn and Fe substitution induces significant magnetism, giving place to overall magnetic moments of 4.00 and 5.00 μ_B, respectively, being produced primarily by TM impurities. Moreover, Mn impurity induces the half-metallicity with perfect spin polarization at the Fermi level, while the magnetic semiconductor nature is obtained by Fe substitution. In both cases, perpendicular magnetic anisotropy (PMA) is confirmed through calculating magnetic anisotropy energy. In addition, the ferromagnetic (FM) phase is energetically stable, exhibiting smaller energy than antiferromagnetic (AFM) and ferrimagnetic (FiM) phases. Robust ferromagnetism is achieved by small TM–TM interatomic distance with high Curie temperature up to 1192.19 K. Further separating transition metal impurities will weaken the ferromagnetism, decreasing significantly Curie temperature. Moreover, it is demonstrated also that Mn–Mn separation switches the electronic nature from magnetic semiconductor to half-metallic, meanwhile the half-metallicity is obtained in the cases of Fe doping and Mn/Fe codoping regardless TM–TM separation. Controlling TM–TM separation is also predicted to effectively regulate the system magnetic anisotropy, inducing the PMA-to-IMA (in-plane magnetic anisotropy) switching and *vice verse*. Our findings may introduce efficient doping approaches to get ferromagnetism in arsenene monolayer, which can form promising 2D candidates for selective spintronic applications.

Received 2nd December 2025
Accepted 15th February 2026

DOI: 10.1039/d5na01113b

rsc.li/nanoscale-advances

1 Introduction

Because of their unique physical and chemical properties related to the atomic thickness, two-dimensional (2D) materials play key role in the development of nanoscience and nanotechnology. Special attention has been paid to 2D materials since the successful isolation of graphene from layered graphite.[1] Graphene is one of the most investigated 2D materials due to its promise for diverse applications including electronics and optoelectronics,[2,3] photonics,[4] photovoltaics,[5] catalysis,[6] energy production and storage,[7] biomedicine,[8] among others. However, its energy gap lacking demands developing efficient functionalization methods for the band gap opening. This goal has been successfully achieved by edge engineering[9,10] and surface functionalization.[11,12] Beyond graphene, new 2D semiconductors have been also discovered by forming compounds as transition metal dichalcogenides,[13,14] **IV–IV** compounds,[15,16] **III–V** compounds,[17,18] **IV–VI** compounds,[19,20] among others. In addition, semiconductor nature has been also confirmed by 2D elemental materials with phosphorene (2D conformation of phosphorus) as a representative. Orthorhombic black phosphorene (BP) has high carrier mobility and thickness-tunable band gap,[21,22] giving place to efficient light absorption from invisible up the near-infrared regime.[23] BP-based field effect transistors (FETs) has large ON/OFF ratio up to 10^5 and high mobility up to 1000 $cm^2 V^{-1} s^{-1}$. Blue phosphorene (BlueP) with hexagonal structure also is confirmed as a 2D semiconductor promising for electronic and optoelectronic devices.[24,25] Stimulated by the success of

[a]*Faculty of Fundamental Sciences, Posts and Telecommunications Institute of Technology, Hanoi, Vietnam*
[b]*Center of Scientific Research and Application, Lac Hong University, No.10 Huynh Van Nghe Str, Tran Bien Ward, Dong Nai Province, Vietnam*
[c]*Universidad Nacional Autónoma de México, Centro de Nanociencias y Nanotecnología, Apartado Postal 14, Ensenada, Baja California, Código Postal 22800, Mexico*
[d]*Laboratory for Computational Physics, Institute for Computational Science and Artificial Intelligence, Van Lang University, Ho Chi Minh City, Vietnam*
[e]*Faculty of Mechanical, Electrical, and Computer Engineering, Van Lang School of Technology, Van Lang University, Ho Chi Minh City, Vietnam*
[f]*Institute of Theoretical and Applied Research, Duy Tan University, Ha Noi 100000, Vietnam. E-mail: dominhhoat@duytan.edu.vn*
[g]*School of Engineering and Technology, Duy Tan University, Da Nang 550000, Vietnam*

phosphorene, group-V elemental monolayers have been attracting great interests as novel 2D materials with exceptional semiconductor electronic properties.[26,27]

On the other hand, the accelerated global development of spintronic devices has motivated huge scientific effort devoted to the discovery of new spintronic materials.[28,29] In this regard, the involvement of magnetism in 2D materials becomes one of the most promising solutions.[30,31] It is important mentioning that spintronic applications of most of 2D materials are considerably limited because of their intrinsic nonmagnetic nature, lacking inherent spin polarization. Therefore, it would be desirable developing novel 2D materials exhibiting feature-rich electronic and magnetic properties, using different methods, including defect engineering,[32–35] substitutional doping,[36–39] and surface functionalization.[40–43] Between them, doping with transition metals (TMs) has been widely investigated experimentally and theoretically as a conventional and simply method, along with its effectiveness in originating magnetic characteristics.[44–47] In general, magnetic properties are influenced by the electronic interactions between unpaired TM-d orbital and their environment. Experimentally, researchers have successfully employed chemical vapor deposition[44,48] or ion implantation (filling the vacancies created previously in 2D materials by transition metal atoms)[49] to realize the controllable transition metal doping in 2D materials, which may open the door to make new 2D magnetic systems towards diverse applications.

2D counterpart of arsenic, namely arsenene, has been predicted by Zhang *et al.*,[50] using first-principles calculations. Results demonstrate the semimetal-to-semiconductor transformation when thinning arsenic structure, consequently an indirect gap of 2.49 eV is obtained for one atomic layer. Moreover, the strain-tunable electronic properties also pave solid way for transistors with high ON/OFF ratio, optoelectronic devices, and mechanical sensors.[51,52] Wang *et al.*[53] have found the non-trivially topological state in arsenene monolayer at tensile strain larger than 11.14%, which is derived from the s–p band inversion. Point defects in arsenene monolayer have been also studied by Liang *et al.*,[54] which can tune the monolayer band gap or introduce strongly local magnetic moments. Arsenene monolayer has been also predicted as outstanding 2D anode material for metal-ion batteries.[55,56] Experimental evidence of arsenene monolayer has been obtained by Shah *et al.*,[57] where characterizations provide a lattice constant of 3.6 Å that is in good agreement with theoretical predictions. Various groups has proposed doping with atomic impurities and organic molecules to modulate the physical properties of arsenene monolayer.[58,59]

In this work, we investigate systematically the effects of transition metal (TM = Mn and Fe) impurities on the electronic and magnetic properties of arsenene monolayer. It is anticipated that the proposed doping approaches can overcome the magnetism lacking of arsenene monolayer. Specifically, transition metal impurities lead to the emergence of the ferromagnetism, in which TM atoms exhibit the parallel spin coupling. Moreover, feature-rich half-metallic and magnetic semiconductor natures are selectively obtained depending on the doping configuration. Our findings contribute to the research effort in searching for novel 2D spintronic materials.

2 Computational details

Within the framework of density functional theory (DFT),[60] our first-principles calculations are based on the projector augmented wave (PAW) method as implemented in Vienna *ab initio* simulation package (VASP).[61,62] Perdew–Burke–Ernzerhof

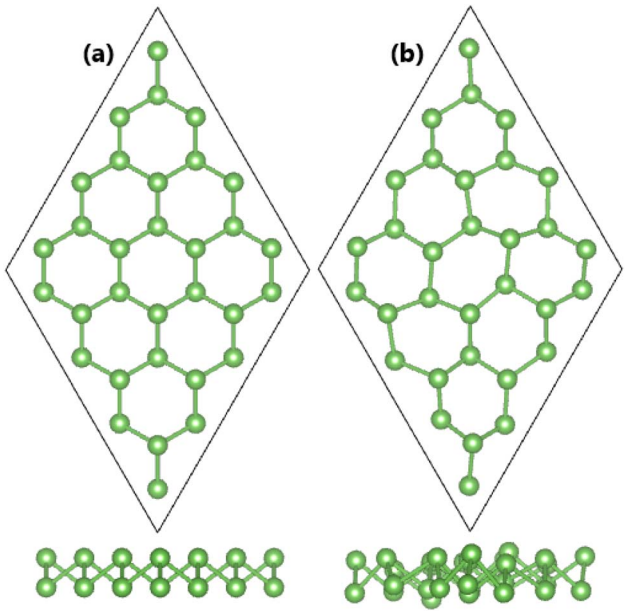

Fig. 1 Atomic structure of arsenene monolayer in a 4 × 4 × 1 supercell: (a) at equilibrium and (b) after 5 ps of AIMD simulations.

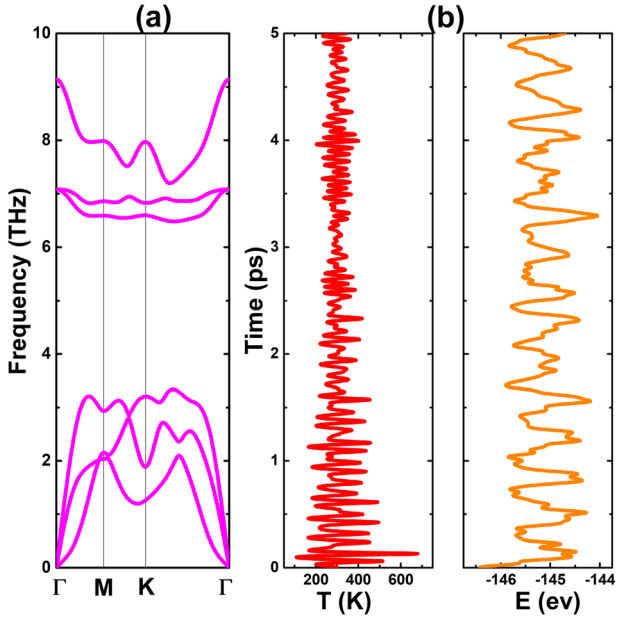

Fig. 2 (a) Phonon dispersion curves and (b) fluctuation of temperature (*T*) and energy (*E*) from AIMD simulations of arsenene monolayer.

functional within the generalized gradient approximation (GGA-PBE) is used in our research for the treatment of exchange–correlation potential.[63] For 3d electrons of transition metals, it will be flawed not considering their high correlation effects that may play important role on the system magnetism. Therefore, DFT + U method is adopted,[64] using an effective Hubbard parameter $U_{\text{eff}} = 4$ eV for both transition metals, which has been applied successfully in previous studied.[65,66] In all calculations, cutoff energy of 500 eV is set to truncate plane-wave basis set. For self-consistent iterations, energy convergence is achieved after satisfying the criterion of 1×10^{-6} eV. All the structure models are relaxed employing the conjugate gradient method, where residual forces are set to be less than 1×10^{-2} eV Å^{-1}. Monkhorst–Pack special k-point grids are generated to sample Brillouin zone.[67] Specifically, $20 \times 20 \times 1$ size is generated for arsenene unit cell, while $4 \times 4 \times 1$ grid is applied for the doped arsenene systems. The monolayer systems considered in this work are modeled through keeping the interactions between adjacent slabs negligible, which is reached by inserting a vacuum gap more than 15 Å.

To simulate the transition metals doping in arsenene monolayer, a $4 \times 4 \times 1$ supercell is generated. Formation energy E_f of the doped arsenene systems is calculated using following expression:

$$E_f = \frac{E(n\text{TM@am}) - E(\text{am}) + n\mu_{\text{As}} - n\mu_{\text{TM}}}{n} \quad (1)$$

where $E(n$TM@am$)$ and E(am) are total energy of the nTM-doped and pristine arsenene monolayer; n is number of transition metal impurities; μ_{As} and μ_{TM} denote chemical potential of As and TM atoms, respectively. Then, their cohesive energy E_c is also computed as follows:

$$E_c = \frac{E(n\text{TM@am}) - (32-n)E(\text{As}) - nE(\text{TM})}{32} \quad (2)$$

herein E(As) and E(TM) are total energy of an isolated As and TM atom, respectively.

Since transition metal impurities leads to the emergence of magnetism in arsenene monolayer, it is important studying magnetic anisotropy that allows designing new magnetic 2D materials for specific applications. Herein, the magnetic anisotropy energy (MAE) is determined by considering the system energy with in-plane x – and perpendicular z – easy magnetization directions as follows:

$$\text{MAE} = E_x - E_z \quad (3)$$

In addition, Curie temperature of the ferromagnetic systems is estimated using mean-field approximation as follows:

$$T_C = \frac{-2\Delta E}{3Nk_B} \quad (4)$$

where ΔE denotes the difference in energy of FM and AFM states; k_B is Boltzmann constant; and N refers to number of TM atoms in the supercell.

3 Results and discussion

3.1 Structural and electronic properties of arsenene monolayer

Before investigating the effects of doping, the structural and electronic properties of arsenene monolayer are studied. Fig. 1a shows the optimized atomic structure of arsenene monolayer in $4 \times 4 \times 1$ supercell with 32 As atoms. Note that arsenene adopts the silicene-like structure, in which As atoms are situated in a buckled honeycomb-like lattice. A unit cell of this 2D material contains 2 As atoms, whose equilibrium state is characterized by following parameters: (1) lattice constant $a = 3.61$ Å; (2) chemical bond length $d_{\text{As–As}} = 2.51$ Å; (3) interatomic angle $\angle\text{AsAsAs} = 91.96°$; and (4) buckling height $\Delta_{\text{As–As}} = 1.40$ Å.

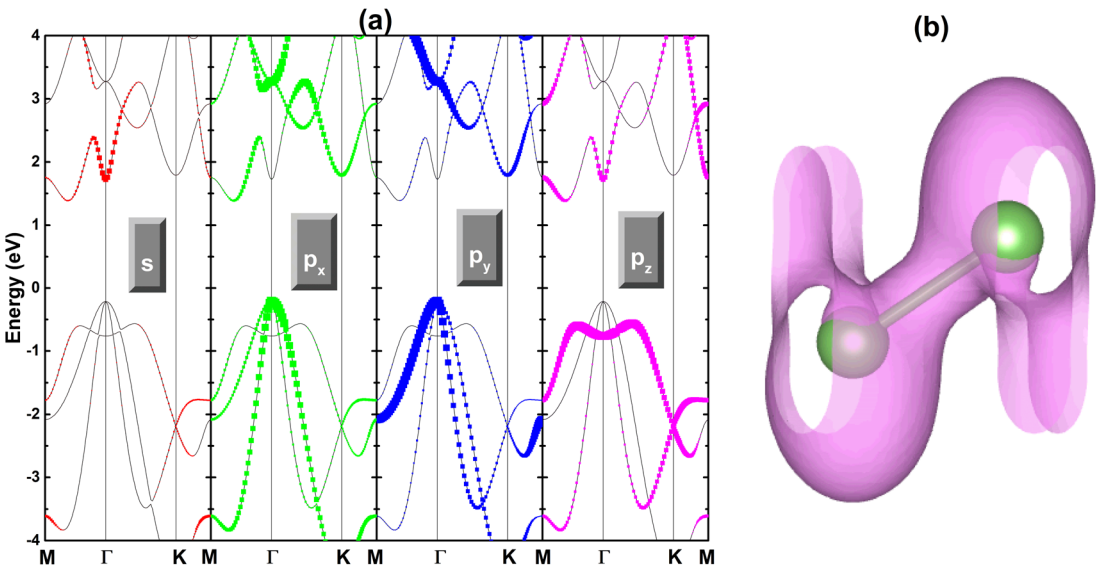

Fig. 3 (a) Orbital-decomposed band structure (the Fermi level is set to 0 eV) and (b) electron localization function (iso-surface value: 0.666 e Å^{-3}).

These results are validated by being in good agreement with previous studies.[68] Then, the dynamical, thermal, and mechanical stability of arsenene monolayer structure is examined as follow:

• Phonon dispersive spectra are calculated using density functional perturbation theory (DFPT) method as implemented in PHONOPY code,[69] which examines the response of system (modeled by a 5 × 5 × 1 supercell) to small perturbation. Results are plotted in Fig. 2a, which show no nonphysical imaginary frequency in entire spectra. This absence indicates that arsenene monolayer is dynamically stable.

• *Ab initio* molecular dynamic (AIMD) simulations are carried out to verify thermal stability of arsenene monolayer, using Nose–Hoover thermostat[70,71] and canonical ensemble at 300 K. Final atomic structure is displayed in Fig. 1b, which shows small displacements of As atoms from their equilibrium sites. Importantly, initial atomic arrangement is well preserved without significant distortions after 5 ps of AIMD simulations. In addition, temperature and total energy exhibit small recovering fluctuations as displayed in Fig. 2b. Therefore, it is safe to conclude that arsenene monolayer is thermally stable.

• Using energy-strain analysis, elastic constants C_{11} and C_{12} of arsenene mnoolayer are calculated to be 53.155 and 9.525 N m^{-1}, respectively. Previously, it has been established that 2D systems with hexagonal symmetry are stable if and only if their elastic constants satisfy following criteria:[72] $C_{11} > 0$ and $C_{11} > |C_{12}|$. Therefore, it can be concluded that arsenene monolayer is mechanically stable considering that its elastic constants follow the stability criteria.

Fig. 3a shows the calculated orbital-decomposed band structure of arsenene monolayer. From the figure, one can see the highest valence band energy point at Γ point and lowest conduction band energy point along $M - \Gamma$ path, asserting the indirect-gap semiconductor nature of arsenene monolayer. According to our calculations, a band gap of 1.60 eV is obtained, which consists well with previous studies.[73] The forbidden energy region is found between upper valence band part formed by As-$p_{x,y}$ states and lower conduction band part originated mainly from As-s – p_x – p_z states. In the considered energy range, As-s and As-p orbitals show significant hybridization that determines the electronic properties of arsenene monolayer. The electronic hybridization generates covalent character of As–As bond. Covalent bond is also confirmed by the electron localization function of arsenene monolayer illustrated in Fig. 3b, where electrons are concentrated mainly at As–As bridge regions without clear directionality.

3.2 Effects of doping with single transition metal

In this part, we investigate the effects of single transition metal impurities (1TM = 1Mn and 1Fe) on the arsenene monolayer electronic and magnetic properties. 1TM-doped arsenene systems are denoted by 1TM@am. Our results provide formation energies of 0.68 and 1.89 eV per atom for 1Mn@am and 1Fe@am systems, respectively. Note that Mn doping in arsenene monolayer is energetically more favorable than Fe doping, requiring less additional energy. Moreover, these

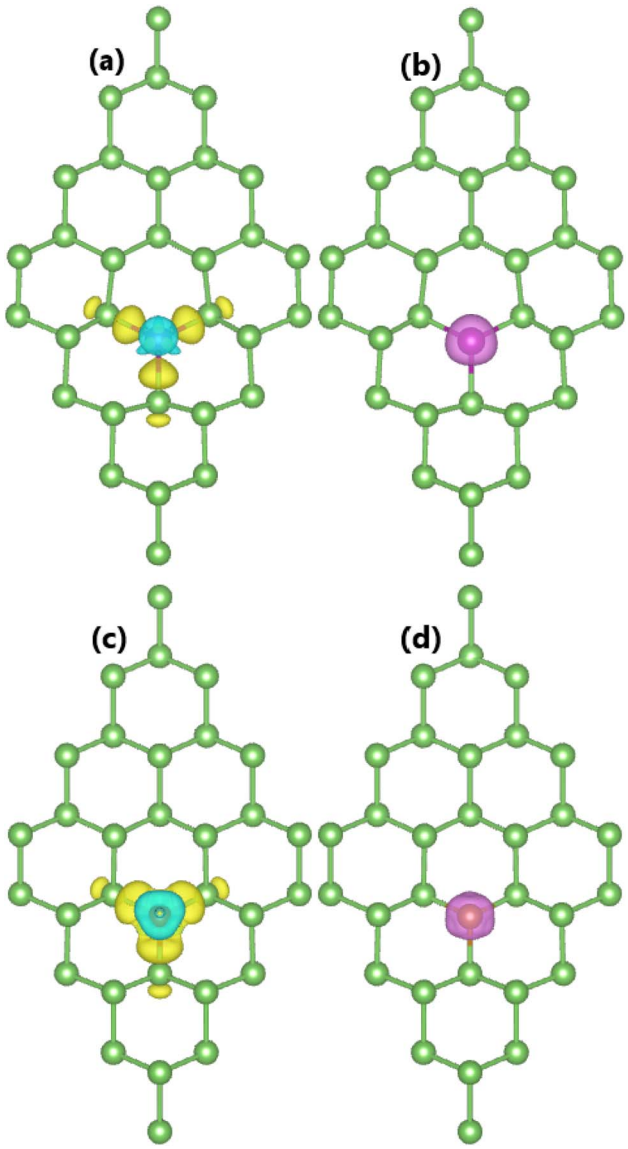

Fig. 4 Charge density difference (iso-surface value: 0.005 e $Å^{-3}$; yellow iso-surfaces: charge accumulation; aqua iso-surfaces: charge depletion) and spin density (iso-surface value: 0.02 e $Å^{-3}$) in (a and b) 1Mn- and (c and d) 1Fe-doped arsenene monolayer.

Table 1 Difference of energy between FM and AFM states ΔE (meV), total magnetic moment M_t (μ_B), magnetic anisotropy energy MAE (μeV), and spin-dependent energy gap (eV; spin-up/spin-down gaps; M = metallic) of different doped arsenene monolayer systems

	ΔE	M_t	MAE	E_g
1Mn@am		4.00	351.47	M/1.56
1Fe@am		5.00	557.46	1.02/0.99
2Mn-1@am	−308.06	8.00	117.38	0.18/1.03
2Mn-2@am	−38.48	8.00	−2769.48	M/1.49
2Fe-1@am	−120.18	6.00	−416.71	M/0.95
2Fe-2@am	−71.04	7.90	1389.5	M/0.88
MnFe-1@am	−222.46	7.00	−407.84	M/1.00
MnFe-2@am	−52.38	9.00	1528.28	M/0.62

systems have negative cohesive energies of −2.99 and −3.03 eV per atom, respectively, which suggest good structural-chemical stability of the doped arsenene systems. To investigate the interactions between TM atoms and their neighboring As atoms, charge density difference $\Delta\rho$ in 1TM@am systems is calculated using following expression: $\Delta\rho = \rho(\text{1TM@am}) - \rho(\text{am}) - \rho(\text{TM})$, where ρ(1TM@am), ρ(am), and ρ(TM) denote charge density of the doped arsenene system, bare arsenene system, and single TM atom, respectively, which are calculated from self-consistent iterations. $\Delta\rho$ results are illustrated in Fig. 4a and c, in which yellow and aqua iso-surfaces are employed to display the charge enrichment and charge depletion, respectively. From the figures, it can be seen that TM impurities deplete charge, meanwhile charge accumulation of their nearest neighboring As atoms is confirmed. Further, Bader charge analysis asserts the charge transfer of 0.81 and 0.51e from Mn and Fe impurities to the host arsenene monolayer, respectively. This feature is a result of the more electronegative nature of As atom that attracts charge of TM atoms.

The results of electronic and magnetic properties are summarized in Table 1. The incorporation of Mn and Fe atoms into arsenene monolayer lattice induces spin polarization, producing significant magnetism. It is found that the nonmagnetic state is less favorable in both 1Mn@am and 1Fe@am systems, exhibiting energy differences of 3.56 and 1.86 eV larger than the magnetic state, respectively, confirming the emergence of magnetism. From our spin-polarized calculations, overall magnetic moments of 4.00 and 5.00 μ_B are obtained for 1Mn@am and 1Fe@am systems, respectively. Further analyzing local magnetic moments, it is found that magnetic moments are originated primarily from TM atoms with large local values of 4.33 and 3.52 μ_B of Mn and Fe atoms, respectively, meanwhile the contribution from the host As atoms is negligible. The atomic contribution is also demonstrated by spin density illustrated in Fig. 4b and d, which show that spin polarization is produced mainly at doping sites as confirmed by large iso-surfaces. In addition, positive MAE values of 351.47 and 557.46 μeV are obtained for 1Mn@am and 1Fe@am systems, respectively, confirming their perpendicular magnetic

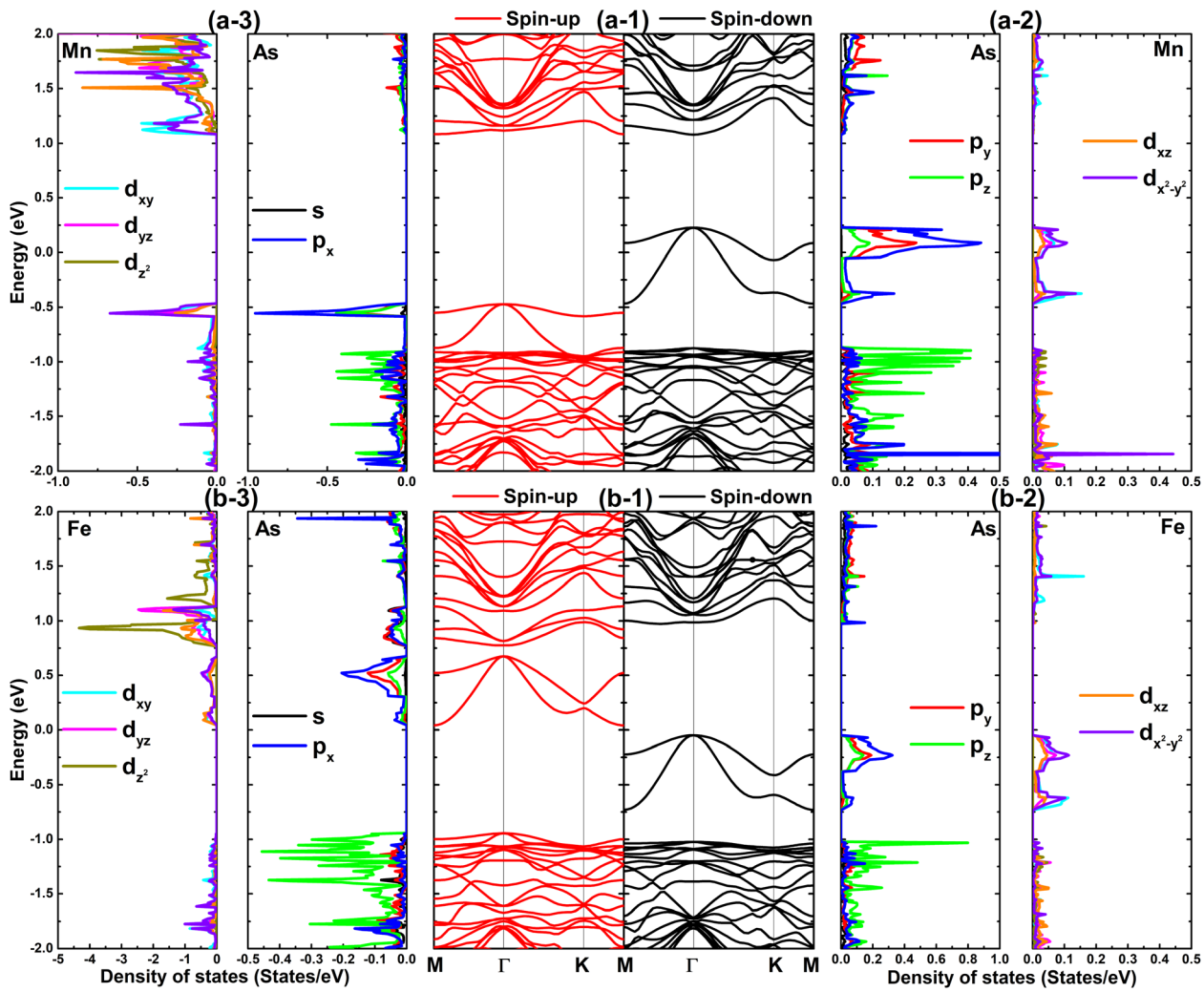

Fig. 5 Spin-resolved band structure and projected density of states (transition metal impurity and its nearest neighboring As atoms) of (a-1–3) 1Mn- and (b-1–3) 1Fe-doped arsenene monlayer (the Fermi level is set to 0 eV).

anisotropy (PMA) that is desirable for Magnetoresistive Random-Access Memory (MRAM) fabrication because of great density and thermal stability.

Fig. 5 shows the calculated spin-polarized band structures (BSs) and projected density of states of 1TM@am systems (PDOS spectra of TM impurities and their nearest neighboring As atoms). The figure shows new mid-gap subbands in both spin states with strong spin polarization in the upper valence band part and lower conduction band part. BSs profiles assert the half-metallicity of 1Mn@am system with perfect spin polarization at the Fermi level, in which semiconductor spin state has an energy gap of 1.56 eV. In this case, Mn-3d and As-4p orbitals determine the electronic properties by forming the energy subbands around the Fermi level. Specifically, spin-up metallic character can be attributed to the interactions of As-$p_{x,y,z}$ and Mn-$d_{xy} - d_{yz} - d_{xz} - d_{x^2-y^2}$ states. Similarly, new mid-gap subbands are also generated by Fe doping to regulate the 1Fe@am system electronic properties. Unlike previous case, there is no overlapping between mid-gap subbands and the Fermi level in both spin states, such that 1Fe@am system can be classified as a 2D magnetic semiconductor material. This difference can be attributed to the dissimilar valence electronic configuration of TM atoms (Fe atom has one more valence electron compared to Mn atom) and their electronic interactions (p–d exchange) with neighboring atoms. In 1Fe@am system, spin-up and spin-down energy gaps of 1.02 and 0.99 eV are obtained, respectively. PDOS spectra demonstrate that these values are determined by As-$p_{x,y,z}$ and Fe-$d_{xy} - d_{yz} - d_{xz} - d_{x^2-y^2}$

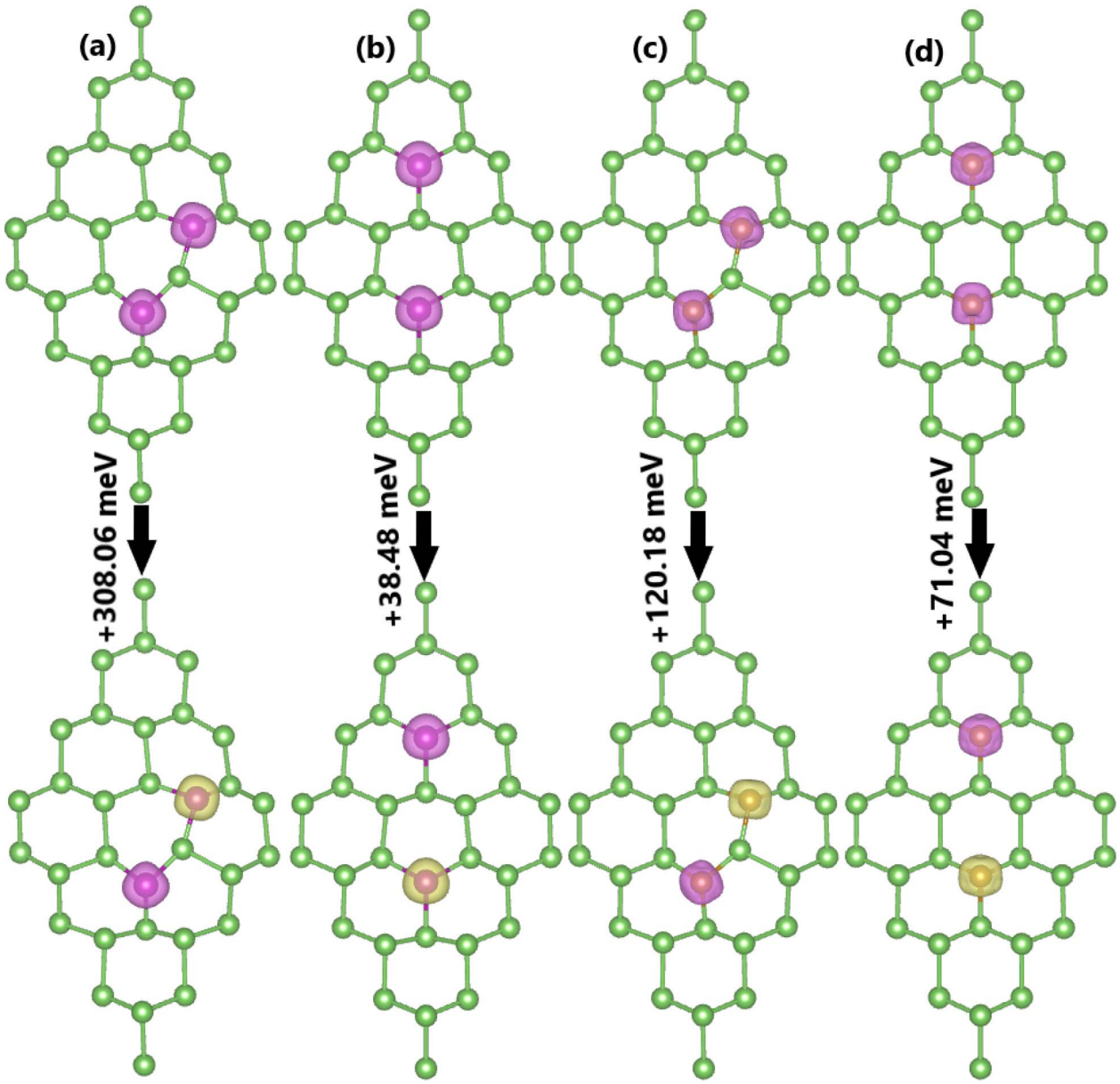

Fig. 6 Spin density (iso-surface value: 0.02 e Å^{-3}) and energy of magnetic phase transition in (a) 2Mn-1-, (b) 2Mn-2-, (c) 2Fe-1-, and (d) 2Fe-2-doped arsenene monolayer.

states that produce mainly the mid-gap subbands in both spin configurations.

3.3 Spin alignment in arsenene monolayer doped transition metal

Now, we determine the magnetic phase in TM-doped arsenene monolayer by assessing the spin coupling between TM impurities that have been proven to produce mainly the system magnetism. Specifically, parallel spin and antiparallel spin configurations are considered, which represent the ferromagnetic (FM) and antiferromagnetic (AFM) phases, respectively. Total system energy is calculated for each case, lower energy indicates the phase stability. Two doping configurations, namely 2TM-1 and 2TM-2 (by increasing the distance between TM impurities), are set in the supercell. The doped systems are denoted by 2TM-1@am and 2TM-2@am, respectively. Fig. 6 illustrates the spin density and energy of magnetic phase transition. Our calculations assert the stability of FM state in all four cases, which has lower energy than AFM state with difference of 308.06 meV for 2Mn-1@am system, 38.48 meV for 2Mn-2@am system, 120.18 meV for 2Fe-1@am system, and 71.04 meV for 2Fe-2@am system. Applying eqn (4), Curie temperatures of 1192.19, 148.92, 465.10, and 274.92 K are obtained for 2Mn-1@am, 2Mn-2@am, 2Fe-1@am, and 2Fe-2@am systems, respectively. Since the mean-field approximation (MFA) generally overestimates Curie temperature because of the inaccurate description of the percolation effects, an empirical relation has been proposed to calculate reliably the lower limit of this parameter, which is defined by: $T_C^{empirical} = 0.51 \times T_C^{MFA}$.[74] According to this relation, the mentioned doped arsenene systems may have T_C larger than 608.02, 75.95, 237.201, and 140.21 K, respectively. Note that the ferromagnetism becomes weaker according to increase the interatomic distance between TM atoms. In previous subsection, it was seen strong interaction between As-4p and TM-3d orbitals. Therefore, it is

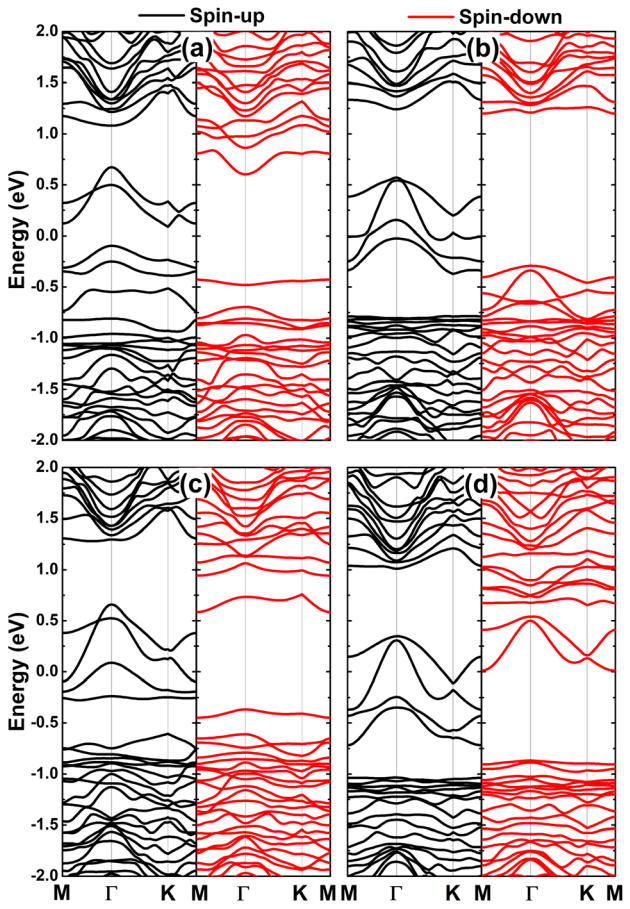

Fig. 7 Spin-resolved band structure of (a) 2Mn-1-, (b) 2Mn-2-, (c) 2Fe-1-, and (d) 2Fe-2-doped arsenene monolayer (the Fermi level is set to 0 eV).

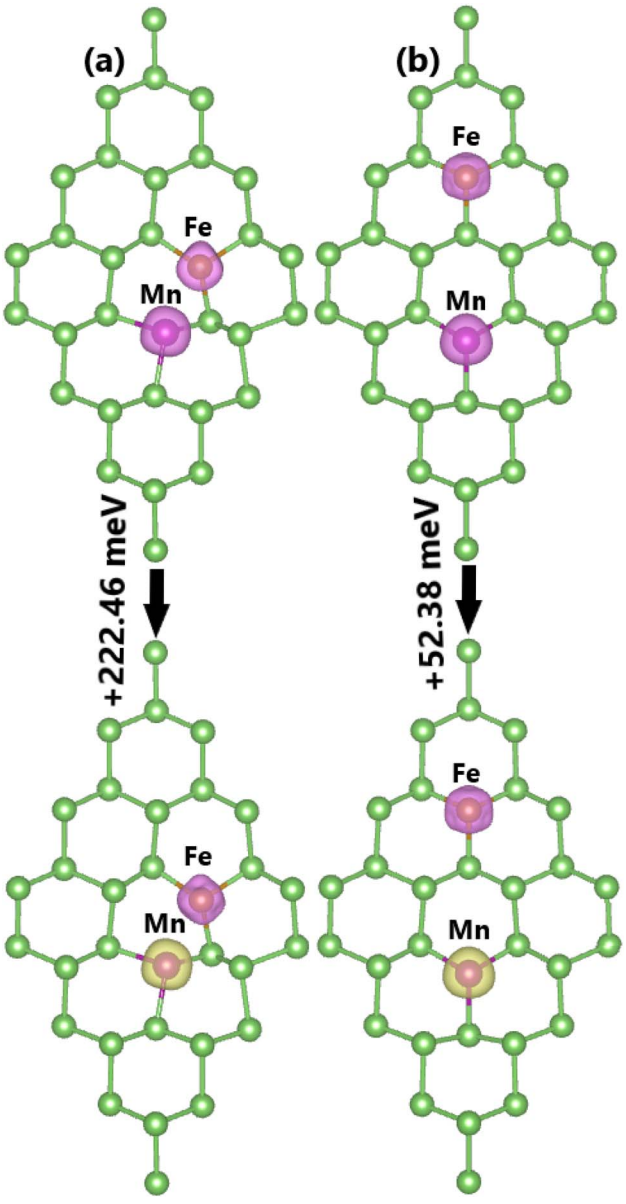

Fig. 8 Spin density (iso-surface value: 0.02 e Å^{-3}) and energy of magnetic phase transition in (a) MnFe-1- and (b) MnFe-2-doped arsenene monolayer.

safe concluding that the ferromagnetism is derived from p–d exchange interactions that are weakened with large TM–TM separation, reducing the FM stability. It is worth mentioning that the considered doped arsenene systems show higher Curie temperature compared to experimental values of the well-known transition-metal-containing VI_3 (46 K)[75] and CrI_3 (45 K)[76] monolayers, suggesting promise of the ferromagnetism for practical applications. The magnetic anisotropy energy of 2Mn-1@am, 2Mn-2@am, 2Fe-1@am, and 2Fe-2@am systems is calculated to be 117.38, −2769.48, −416.71, and 1389.5 μeV, respectively. Note that small Mn–Mn separation induces the PMA, further separating the interatomic distance will induce the PMA-to-IMA switching, opposite effects are obtained for the cases of Fe doping. Therefore, effective control of doping configurations will be useful to selectively functionalize arsenene monolayer for MRAM fabrication and magnetic field sensing (with IMA needed). Results also assert that stronger magnetic anisotropy is obtained by large TM–TM separation as suggested by large MAE values.

Fig. 7 shows the spin-resolved band structures of 2TM-1@am and 2TM-2@am systems in FM phase. It can be noted multiple mid-gap energy subbands that determine the electronic nature. Specifically, 2Mn-1@am system exhibits the ferromagnetic semiconductor nature with spin-up and spin-down energy gaps of 0.18 and 1.03 eV, respectively. Further separating Mn–Mn atoms will switch the electronic nature to half-metallic of 2Mn-2@am system, considering the metallization of spin-up state. In latter case, spin-down state has an energy gap of 1.49 eV. Meanwhile, the ferromagnetic half-metallicity is obtained by Fe doping regardless Fe–Fe separation, where spin-down energy gap of 2Fe-1@am and 2Fe-2@am systems is calculated to be 0.95 and 0.88 eV, respectively.

3.4 Effects of Mn and Fe codoping

Now, effects of Mn and Fe codoping in arsenene monolayer are investigated. We denote the doped systems by MnFe-1@am and MnFe-2@am with increasing the interatomic distance between transition metals. FM state with parallel Mn/Fe spin coupling and FiM (ferrimagnetic) state with antiparallel Mn/Fe spin coupling are considered. Fig. 8 illustrates spin density along with difference in energy of FM and FiM phases. Our calculations assert the stability of FM phase that has smaller energy than FiM phase with difference of 222.46 meV for MnFe-1@am and 52.38 meV for MnFe-2@am systems. These values allow deriving Curie temperatures of 860.92 and 202.71 K from the mean-field approximation, respectively. In addition, lower T_C limits of 439.07 and 103.38 K are obtained from the empirical relation, respectively. Similar to previous cases of doping, the decrease of Curie temperature suggests the reduction of FM phase stability according to further separating transition metal impurities. Moreover, Mn–Fe distance also influences considerably on the system magnetic anisotropy. Specifically, MAE values of −407.84 and 1528.28 μeV are obtained for MnFe-1@am and MnFe-2@am systems, respectively, confirming the IMA-to-PMA switching induced by controlling the doping configuration.The spin-resolved band structures of MnFe-1@am and MnFe-2@am systems are displayed in Fig. 9. Regardless

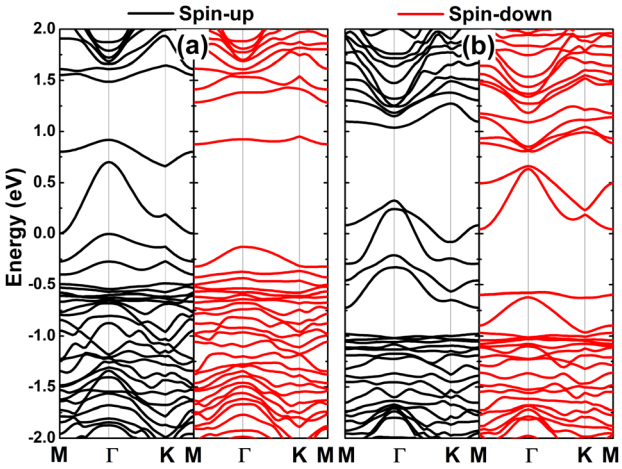

Fig. 9 Spin-resolved band structure of (a) MnFe-1- and (b) MnFe-2-doped arsenene monolayer (the Fermi level is set to 0 eV).

Mn–Fe distance, the ferromagnetic half-metallicity is obtained, giving place to 100% spin polarization at the Fermi level. In these cases, energy gaps of semiconductor spin-down state are 1.00 and 0.62 eV, respectively. These feature-rich electronic and magnetic properties also suggest the prospect of the codoped arsenene systems for selective spintronic applications.

4 Conclusions

In summary, effects of transition metals doping on the arsenene monolayer electronic and magnetic properties have been systematically investigated using first-principles calculations. Pristine arsenene monolayer has good stability, exhibiting indirect-gap semiconductor nature without intrinsic magnetism. Strong electronic hybridization gives place to covalent As–As chemical bond. Significant magnetism is induced by TM doping, where impurities transfer charge to the host monolayer and produce primarily the magnetism of the doped systems. Moreover, the interactions between As-$p_{x,y,z}$ and TM-$d_{xy} - d_{yz} - d_{xz} - d_{x^2-y^2}$ states states produce multiple mid-gap subbands in both spin configurations, originating the feature-rich electronic and magnetic properties. p–d exchange interactions also originate robust ferromagnetism with high Curie temperature between 465.10 and 1192.19 K. However, this parameter is reduced significantly by further increasing TM–TM separation, suggesting the ferromagnetism weakening. Depending on TM–TM distance, either half-metallic nature with perfect spin polarization at the Fermi level or magnetic semiconductor nature with both semiconductor spin states is obtained. Moreover, the magnetic anisotropy can be also switched by varying TM–TM separation, which is crucial to design arsenene monolayer for either MRAM fabrication or magnetic field sensing. It has been found also that large TM–TM distance is favorable for the stability of magnetic anisotropy, which is suggested by large MAE values. The obtained results provide important insights into the effects of TMs impurities in arsenene monolayer, paving solid way to functionalize this 2D

material towards selective spintronic applications by effectively controlling TM–TM separation.

Conflicts of interest

The authors declare that they have no known competing financial interests or personal relationships that could have appeared to influence the work reported in this paper.

Data availability

Data will be provided under requesting to authors.

Acknowledgements

Calculations were performed in DGCTIC-UNAM Supercomputing Center (projects LANCAD-UNAM-DGTIC-368).

References

1 K. S. Novoselov, A. K. Geim, S. V. Morozov, D.-E. Jiang, Y. Zhang, S. V. Dubonos, I. V. Grigorieva and A. A. Firsov, Electric field effect in atomically thin carbon films, *science*, 2004, **306**(5696), 666–669.
2 H. Chang and H. Wu, Graphene-based nanomaterials: Synthesis, properties, and optical and optoelectronic applications, *Adv. Funct. Mater.*, 2013, **23**(16), 1984–1997.
3 P. Avouris and F. Xia, Graphene applications in electronics and photonics, *MRS Bull.*, 2012, **37**(12), 1225–1234.
4 F. Bonaccorso, Z. Sun, T. Hasan and A. C. Ferrari, Graphene photonics and optoelectronics, *Nat. Photonics*, 2010, **4**(9), 611–622.
5 S. Das, D. Pandey, J. Thomas and T. Roy, The role of graphene and other 2D materials in solar photovoltaics, *Adv. Mater.*, 2019, **31**(1), 1802722.
6 C. Huang, C. Li and G. Shi, Graphene based catalysts, *Energy Environ. Sci.*, 2012, **5**(10), 8848–8868.
7 D. A. Brownson, D. K. Kampouris and C. E. Banks, An overview of graphene in energy production and storage applications, *J. Power Sources*, 2011, **196**(11), 4873–4885.
8 L. Feng and Z. Liu, Graphene in biomedicine: opportunities and challenges, *Nanomedicine*, 2011, **6**(2), 317–324.
9 M. Y. Han, B. Özyilmaz, Y. Zhang and P. Kim, Energy band-gap engineering of graphene nanoribbons, *Phys. Rev. Lett.*, 2007, **98**(20), 206805.
10 Y.-W. Son, M. L. Cohen and S. G. Louie, Energy gaps in graphene nanoribbons, *Phys. Rev. Lett.*, 2006, **97**(21), 216803.
11 J. E. Johns and M. C. Hersam, Atomic covalent functionalization of graphene, *Acc. Chem. Res.*, 2013, **46**(1), 77–86.
12 H. Zhang, E. Bekyarova, J.-W. Huang, Z. Zhao, W. Bao, F. Wang, R. C. Haddon and C. N. Lau, Aryl functionalization as a route to band gap engineering in single layer graphene devices, *Nano Lett.*, 2011, **11**(10), 4047–4051.
13 K. F. Mak and J. Shan, Photonics and optoelectronics of 2D semiconductor transition metal dichalcogenides, *Nat. Photonics*, 2016, **10**(4), 216–226.
14 S. Manzeli, D. Ovchinnikov, D. Pasquier, O. V. Yazyev and A. Kis, 2D transition metal dichalcogenides, *Nat. Rev. Mater.*, 2017, **2**(8), 1–15.
15 T.-Y. Lü, X.-X. Liao, H.-Q. Wang and J.-C. Zheng, Tuning the indirect–direct band gap transition of SiC, GeC and SnC monolayer in a graphene-like honeycomb structure by strain engineering: a quasiparticle GW study, *J. Mater. Chem.*, 2012, **22**(19), 10062–10068.
16 C. V. Ha, L. Ha, D. K. Nguyen, D. T. Anh, J. Guerrero-Sanchez, D. Hoat, *et al.*, First-principles study of SiC and GeC monolayers with adsorbed non-metal atoms, *RSC Adv.*, 2023, **13**(22), 14879–14886.
17 Y. Chen, J. Liu, M. Zeng, F. Lu, T. Lv, Y. Chang, H. Lan, B. Wei, R. Sun, J. Gao, *et al.*, Universal growth of ultra-thin III–V semiconductor single crystals, *Nat. Commun.*, 2020, **11**(1), 3979.
18 T. Suzuki, Theoretical discovery of stable structures of group III-V monolayers: The materials for semiconductor devices, *Appl. Phys. Lett.*, 2015, **107**(21), 213105.
19 C. Kamal, A. Chakrabarti and M. Ezawa, Direct band gaps in group IV-VI monolayer materials: Binary counterparts of phosphorene, *Phys. Rev. B*, 2016, **93**(12), 125428.
20 K. Ren, X. Ma, X. Liu, Y. Xu, W. Huo, W. Li and G. Zhang, Prediction of 2D IV–VI semiconductors: auxetic materials with direct bandgap and strong optical absorption, *Nanoscale*, 2022, **14**(23), 8463–8473.
21 L. Li, Y. Yu, G. J. Ye, Q. Ge, X. Ou, H. Wu, D. Feng, X. H. Chen and Y. Zhang, Black phosphorus field-effect transistors, *Nat. Nanotechnol.*, 2014, **9**(5), 372–377.
22 H. Guo, W. Chu, O. V. Prezhdo, Q. Zheng and J. Zhao, Strong modulation of band gap, carrier mobility and lifetime in two-dimensional black phosphorene through acoustic phonon excitation, *J. Phys. Chem. Lett.*, 2021, **12**(16), 3960–3967.
23 M. Zhang, G. M. Biesold and Z. Lin, A multifunctional 2D black phosphorene-based platform for improved photovoltaics, *Chem. Soc. Rev.*, 2021, **50**(23), 13346–13371.
24 W. Zhang, H. Enriquez, Y. Tong, A. Bendounan, A. Kara, A. P. Seitsonen, A. J. Mayne, G. Dujardin and H. Oughaddou, Epitaxial synthesis of blue phosphorene, *Small*, 2018, **14**(51), 1804066.
25 B. Ghosh, S. Nahas, S. Bhowmick and A. Agarwal, Electric field induced gap modification in ultrathin blue phosphorus, *Phys. Rev. B*, 2015, **91**(11), 115433.
26 J. Lee, W.-C. Tian, W.-L. Wang and D.-X. Yao, Two-dimensional pnictogen honeycomb lattice: structure, on-site spin-orbit coupling and spin polarization, *Sci. Rep.*, 2015, **5**(1), 11512.
27 P. K. Roy, J. Luxa and Z. Sofer, Emerging pnictogen-based 2D semiconductors: sensing and electronic devices, *Nanoscale*, 2020, **12**(19), 10430–10446.
28 X. Li and J. Yang, First-principles design of spintronics materials, *Natl. Sci. Rev.*, 2016, **3**(3), 365–381.

29 V. Ivanov, T. Aminov, V. Novotortsev and V. Kalinnikov, Spintronics and spintronics materials, *Russ. Chem. Bull.*, 2004, **53**(11), 2357–2405.
30 E. C. Ahn, 2D materials for spintronic devices, *npj 2D Mater. Appl.*, 2020, **4**(1), 17.
31 Y. P. Feng, L. Shen, M. Yang, A. Wang, M. Zeng, Q. Wu, S. Chintalapati and C.-R. Chang, Prospects of spintronics based on 2D materials, *Wiley Interdiscip. Rev.: Comput. Mol. Sci.*, 2017, **7**(5), e1313.
32 R. Sanikop and C. Sudakar, Tailoring magnetically active defect sites in MoS_2 nanosheets for spintronics applications, *ACS Appl. Nano Mater.*, 2019, **3**(1), 576–587.
33 R. Babar and M. Kabir, Transition metal and vacancy defect complexes in phosphorene: a spintronic perspective, *J. Phys. Chem. C*, 2016, **120**(27), 14991–15000.
34 M. Y. Khan, T. Usman, A. Ilyas, A. Hassan, U. Younis, A. Ullah, S. A. Ahmad and A. Al Souwaileh, Electronic, optical, and magnetic properties of defect-engineered 1T-PdS_2 monolayer: A first-principles investigation, *Mater. Sci. Semicond. Process.*, 2025, **187**, 109144.
35 S. Chakraborty, M. Ramesh and M. K. Niranjan, Defect-engineered magnetism in conventional and Janus 2D vdW semiconducting monolayers: Benchmark insights from first-principles investigation, *J. Magn. Magn. Mater.*, 2025, 173714.
36 Y. Wang and J. Yi, Ferromagnetism in two-dimensional materials *via* doping and defect engineering, in. *Spintronic 2D Materials*, Elsevier, 2020, pp. 95–124.
37 S. Feng, Z. Lin, X. Gan, R. Lv and M. Terrones, Doping two-dimensional materials: ultra-sensitive sensors, band gap tuning and ferromagnetic monolayers, *Nanoscale Horiz.*, 2017, **2**(2), 72–80.
38 M. S. Pervez, M. F. Hossain, M. Jubair, M. A. H. Shah, M. Nuruzzaman and M. Nahid, The electronic and magnetic properties of Cr-doped ZnO monolayer at higher percentage by first principles calculations, *Mater. Sci. Semicond. Process.*, 2025, **186**, 108999.
39 W. Ma, D. Deng, P. Wang, L. Lin and D. Wang, Magnetic and optical properties of (Mn, Tc) co-doped HfS_2 monolayer: A first-principles study, *Mater. Sci. Eng. B*, 2026, **323**, 118815.
40 K. Ren, K. Wang and G. Zhang, Atomic adsorption-controlled magnetic properties of a two-dimensional (2D) janus monolayer, *ACS Appl. Electron. Mater.*, 2022, **4**(9), 4507–4513.
41 D. K. Nguyen, T. V. Vu and D. Hoat, Antiferromagnetic ordering in the TM-adsorbed AlN monolayer (TM= V and Cr), *RSC Adv.*, 2022, **12**(26), 16677–16683.
42 B. Xu, W. Zhao, Y. Yan, C. Qian, M. Yang, Q. Yang, L. Shi, Y. Wang, Z. Cao and L. Yi, Prediction of electronic structure and magnetic properties of monolayer MoTeSe adsorbing transition metal elements, *J. Appl. Phys.*, 2025, **138**(8), 084301.
43 W. Zhao, B. Xu, C. Qian, M. Yang, D. Zhou, Y. Wang, Z. Cao and L. Yi, Magnetic properties of transition elements adsorbed B_2S_2 monolayers, *Chem. Phys.*, 2025, 112769.
44 D. Shen, B. Zhao, Z. Zhang, H. Zhang, X. Yang, Z. Huang, B. Li, R. Song, Y. Jin, R. Wu, *et al.*, Synthesis of group VIII magnetic transition-metal-doped monolayer $MoSe_2$, *ACS Nano*, 2022, **16**(7), 10623–10631.
45 X.-L. Fan, Y.-R. An and W.-J. Guo, Ferromagnetism in transitional metal-doped MoS_2 monolayer, *Nanoscale Res. Lett.*, 2016, **11**(1), 154.
46 A. A. Tedstone, D. J. Lewis and P. O'Brien, Synthesis, properties, and applications of transition metal-doped layered transition metal dichalcogenides, *Chem. Mater.*, 2016, **28**(7), 1965–1974.
47 J. Gao, Y. D. Kim, L. Liang, J. C. Idrobo, P. Chow, J. Tan, B. Li, L. Li, B. G. Sumpter, T.-M. Lu, *et al.*, Transition-metal substitution doping in synthetic atomically thin semiconductors, *Adv. Mater.*, 2016, **28**(44), 9735–9743.
48 J. Zhou, J. Lin, H. Sims, C. Jiang, C. Cong, J. A. Brehm, Z. Zhang, L. Niu, Y. Chen, Y. Zhou, *et al.*, Synthesis of co-doped MoS_2 monolayers with enhanced valley splitting, *Adv. Mater.*, 2020, **32**(11), 1906536.
49 J. A. Rodríguez-Manzo, O. Cretu and F. Banhart, Trapping of metal atoms in vacancies of carbon nanotubes and graphene, *ACS Nano*, 2010, **4**(6), 3422–3428.
50 S. Zhang, Z. Yan, Y. Li, Z. Chen and H. Zeng, Atomically thin arsenene and antimonene: semimetal–semiconductor and indirect–direct band-gap transitions, *Angew. Chem., Int. Ed.*, 2015, **54**(10), 3112–3115.
51 H. Cao, Z. Yu and P. Lu, Electronic properties of monolayer and bilayer arsenene under in-plain biaxial strains, *Superlattices Microstruct.*, 2015, **86**, 501–507.
52 D. Guo, B. Shao, C. Li and Y. Ma, Theoretical insight into structure stability, elastic property and carrier mobility of monolayer arsenene under biaxial strains, *Superlattices Microstruct.*, 2016, **100**, 324–334.
53 Y.-P. Wang, C.-W. Zhang, W.-X. Ji, R.-W. Zhang, P. Li, P.-J. Wang, M.-J. Ren, X.-L. Chen and M. Yuan, Tunable quantum spin Hall effect *via* strain in two-dimensional arsenene monolayer, *J. Phys. D: Appl. Phys.*, 2016, **49**(5), 055305.
54 X. Liang, S.-P. Ng, N. Ding and C.-M. L. Wu, Characterization of point defects in monolayer arsenene, *Appl. Surf. Sci.*, 2018, **443**, 74–82.
55 H. Benzidi, M. Lakhal, M. Garara, M. Abdellaoui, A. Benyoussef, O. Mounkachi, *et al.*, Arsenene monolayer as an outstanding anode material for (Li/Na/Mg)-ion batteries: density functional theory, *Phys. Chem. Chem. Phys.*, 2019, **21**(36), 19951–19962.
56 X.-J. Ye, G.-L. Zhu, J. Liu, C.-S. Liu and X.-H. Yan, Monolayer, bilayer, and heterostructure arsenene as potential anode materials for magnesium-ion batteries: a first-principles study, *J. Phys. Chem. C*, 2019, **123**(25), 15777–15786.
57 J. Shah, W. Wang, H. M. Sohail and R. Uhrberg, Experimental evidence of monolayer arsenene: an exotic 2D semiconducting material, *2D Materials*, 2020, **7**(2), 025013.
58 Z. Li, W. Xu, Y. Yu, H. Du, K. Zhen, J. Wang, L. Luo, H. Qiu and X. Yang, Monolayer hexagonal arsenene with tunable electronic structures and magnetic properties *via* impurity doping, *J. Mater. Chem. C*, 2016, **4**(2), 362–370.

59 D. Singh, S. K. Gupta, Y. Sonvane and S. Sahoo, Modulating the electronic and optical properties of monolayer arsenene phases by organic molecular doping, *Nanotechnology*, 2017, **28**(49), 495202.
60 W. Kohn and L. J. Sham, Self-consistent equations including exchange and correlation effects, *Phys. Rev.*, 1965, **140**(4A), A1133, DOI: 10.1103/PhysRev.140.A1133.
61 G. Kresse and J. Furthmüller, Efficiency of *ab initio* total energy calculations for metals and semiconductors using a plane-wave basis set, *Comput. Mater. Sci.*, 1996, **6**(1), 15–50, DOI: 10.1016/0927-0256(96)00008-0.
62 G. Kresse and J. Furthmüller, Efficient iterative schemes for *ab initio* total-energy calculations using a plane-wave basis set, *Phys. Rev. B*, 1996, **54**(16), 11169, DOI: 10.1103/PhysRevB.54.11169.
63 J. P. Perdew, K. Burke and M. Ernzerhof, Generalized gradient approximation made simple, *Phys. Rev. Lett.*, 1996, **77**(18), 3865, DOI: 10.1103/PhysRevLett.77.3865.
64 S. L. Dudarev, G. A. Botton, S. Y. Savrasov, C. Humphreys and A. P. Sutton, Electron-energy-loss spectra and the structural stability of nickel oxide: An LSDA+U study, *Phys. Rev. B*, 1998, **57**(3), 1505.
65 B. Wang, Y. Zhang, L. Ma, Q. Wu, Y. Guo, X. Zhang and J. Wang, MnX (X= P, As) monolayers: a new type of two-dimensional intrinsic room temperature ferromagnetic half-metallic material with large magnetic anisotropy, *Nanoscale*, 2019, **11**(10), 4204–4209.
66 S. Pakdel, T. Olsen and K. S. Thygesen, Effect of Hubbard U-corrections on the electronic and magnetic properties of 2D materials: a high-throughput study, *npj Comput. Mater.*, 2025, **11**(1), 18.
67 H. J. Monkhorst and J. D. Pack, Special points for Brillouin-zone integrations, *Phys. Rev. B*, 1976, **13**(12), 5188, DOI: 10.1103/PhysRevB.13.5188.
68 Y. Xu, B. Peng, H. Zhang, H. Shao, R. Zhang and H. Zhu, First-principle calculations of optical properties of monolayer arsenene and antimonene allotropes, *Ann. Phys.*, 2017, **529**(4), 1600152.
69 A. Togo, L. Chaput, T. Tadano and I. Tanaka, Implementation strategies in phonopy and phono3py, *J. Phys. Condens. Matter*, 2023, **35**(35), 353001, DOI: 10.1088/1361-648X/acd831.
70 S. Nosé, A unified formulation of the constant temperature molecular dynamics methods, *J. Chem. Phys.*, 1984, **81**(1), 511–519.
71 W. G. Hoover, Canonical dynamics: Equilibrium phase-space distributions, *Phys. Rev.*, 1985, **31**(3), 1695.
72 F. Mouhat and F.-X. Coudert, Necessary and sufficient elastic stability conditions in various crystal systems, *Phys. Rev. B Condens. Matter*, 2014, **90**(22), 224104.
73 D. Kecik, E. Durgun and S. Ciraci, Stability of single-layer and multilayer arsenene and their mechanical and electronic properties, *Phys. Rev. B*, 2016, **94**(20), 205409.
74 Z. Liu, J. Liu and J. Zhao, YN_2 monolayer: Novel p-state Dirac half metal for high-speed spintronics, *Nano Res.*, 2017, **10**(6), 1972–1979.
75 F. Subhan and J. Hong, Magnetic anisotropy and curie temperature of two-dimensional VI_3 monolayer, *J. Phys.: Condens. Matter*, 2020, **32**(24), 245803.
76 B. Huang, G. Clark, E. Navarro-Moratalla, D. R. Klein, R. Cheng, K. L. Seyler, D. Zhong, E. Schmidgall, M. A. McGuire, D. H. Cobden, *et al.*, Layer-dependent ferromagnetism in a van der Waals crystal down to the monolayer limit, *Nature*, 2017, **546**(7657), 270–273.